LBL-18172
UC-25

Lawrence Berkeley Laboratory

UNIVERSITY OF CALIFORNIA

RECEIVED
LAWRENCE
BERKELEY LABORATORY

OCT 9 1984

LIBRARY AND
DOCUMENTS SECTION

Materials & Molecular Research Division

Presented at the 13th International Conference on Defects and Semiconductors, Coronado, CA, August 12-17, 1984

INFLUENCE OF THE AMORPHOUS-CRYSTALLINE INTERFACE MORPHOLOGY ON DISLOCATION NUCLEATION IN PRE-AMORPHIZED SILICON

T. Sands, J. Washburn, R. Gronsky, W. Maszara, D.K. Sadana, and G.A. Rozgonyi

August 1984

For Reference

Not to be taken from this room

LBL-18172

Prepared for the U.S. Department of Energy under Contract DE-AC03-76SF00098

DISCLAIMER

This document was prepared as an account of work sponsored by the United States Government. While this document is believed to contain correct information, neither the United States Government nor any agency thereof, nor the Regents of the University of California, nor any of their employees, makes any warranty, express or implied, or assumes any legal responsibility for the accuracy, completeness, or usefulness of any information, apparatus, product, or process disclosed, or represents that its use would not infringe privately owned rights. Reference herein to any specific commercial product, process, or service by its trade name, trademark, manufacturer, or otherwise, does not necessarily constitute or imply its endorsement, recommendation, or favoring by the United States Government or any agency thereof, or the Regents of the University of California. The views and opinions of authors expressed herein do not necessarily state or reflect those of the United States Government or any agency thereof or the Regents of the University of California.

INFLUENCE OF THE AMORPHOUS-CRYSTALLINE INTERFACE MORPHOLOGY ON DISLOCATION NUCLEATION IN PRE-AMORPHIZED SILICON

T. Sands*, J. Washburn*, R. Gronsky*, W. Maszara+,
D.K. Sadana+** and G.A. Rozgonyi+**

*Materials and Molecular Research Division
Lawrence Berkeley Laboratory
Berkeley, California 94720

+Materials Engineering Department
North Carolina State University
Raleigh, North Carolina 27650

**Microelectronics Center of North Carolina
Research Triangle Park
North Carolina 27709

Abstract

Cross-sectional high-resolution transmission electron microscopy and secondary-ion mass spectrometry are applied to the characterization of defects formed during rapid thermal annealing of pre-amorphized and subsequently BF_2^+-implanted (100) silicon substrates. The occurrence of "hairpin" dislocations is shown to be directly related to the degree of total disorder (i.e. amorphization) in the transition region between amorphous and crystalline material before annealing. A model for the nucleation and propagation of these dislocations is developed on the basis of the microscopy results. Finally, pre-amorphization conditions which minimize the density of hairpin dislocations are discussed.

Introduction

Implantation of B^+ or BF_2^+ into crystalline silicon results in a boron profile with a pronounced channeling tail (1,2). This channeling

tail puts a lower limit on the achievable junction depth for a given implant energy (3). Thus, the implementation of some means for channeling suppression is desirable when fabricating very shallow ($\lesssim$ 0.1μm) p^+-n junctions. The most effective technique for eliminating boron channeling is amorphization of the silicon surface layer ($\sim$0.2-1 μm) by ion bombardment prior to dopant introduction (2,3). This "pre-amorphization" step is generally accomplished by self-implantation into substrates which are cooled by liquid nitrogen (2-14). More recently, groups at the Microelectronics Center of North Carolina and AT&T Bell Laboratories have explored the use of Ge^+-implantation as an alternative to Si^+-pre-amorphization (9-13).

Following B^+ or BF_2^+ implantation, the silicon substrate must be annealed at temperatures $\gtrsim$550° C to crystallize the amorphous layer by solid-phase epitaxy from the interface between amorphous and crystalline silicon. In an effort to minimize dopant redistribution during annealing, rapid thermal annealing (RTA) with incoherent light has recently been employed (6-14). However, the samples annealed by this technique have been shown to contain as many as three distinct layers of secondary defects (7,8). The origin and annealing behavior of two of these defect layers, the near-surface defects (type III in ref. (7,8)) and the interstitial loops (type I) formed near the original amorphous-crystalline interface have been described in some detail (12-14). However, an additional class of defects (type II) described as "hairpin" (7,8) or "spanning" (9) dislocations has not been thoroughly investigated. These defects may be detrimental to device performance, especially if they span the space-charge layer. Therefore, it is

important to understand the hairpin nucleation process so that the processing conditions which yield hairpin-free p^+-n shallow junctions can be predicted.

In this study, the origin and annealing behavior of hairpin dislocations are investigated with cross-sectional transmission electron microscopy (XTEM) and secondary-ion mass spectrometry (SIMS). It is demonstrated below that the formation of hairpin dislocations is related to the morphology of the transition region between amorphous and crystalline silicon.

Experimental Methods

Pre-amorphization of (100) silicon was accomplished by either triple-energy implantation of Si^+ (300, 150 and 70 keV to doses of 10^{16}, $2x10^{15}$ and $5x10^{15}$ cm^{-2}, respectively) into LN_2-cooled substrates or by single-step Ge^+ implantation (300 keV to doses of $1x10^{15}$ - $1x10^{16}$ cm^{-2}). Implantation of BF_2^+ at 42 keV to a dose of $2x10^{15}$ cm^{-2} provided the shallow boron profile. The boron and fluorine distributions were determined by SIMS (Cameca IMS model 3F) before and after RTA in the temperature range 750-1150°C for 10 seconds. Samples for XTEM were prepared by mechanical polishing and Ar^+ ion milling (5 keV, stage cooled with LN_2). Microscopy was performed with both a Siemens 102 at 100 keV and a JEOL JEM 200-CX at 200 keV.

Results and Discussion

The highest densities (1-5 x 10^8 cm^{-2}) of hairpin dislocations were observed in Si^+-pre-amorphized samples which were implanted with BF_2^+ at (nominal) room temperature. The XTEM images and SIMS data in Fig. 1 show that fluorine is strongly gettered by the tips of hairpin

dislocations and by the interstitial loops. In addition, as the hairpin dislocations move toward the surface during high temperature annealing, the shoulder in the fluorine profile moves also. Although the fluorine-defect interaction is evidently quite strong, the presence of fluorine is not necessary for the nucleation of hairpins. For example, Si^+-pre-amorphized samples which were not implanted with BF_2^+ were found to contain significant densities ($0.5\text{-}5\times10^7 cm^{-2}$) of hairpin dislocations.

In order to simulate heating effects during BF_2^+ implantation, Si^+-pre-amorphized samples were given furnace heat treatments (250-350 °C, 1 h) prior to RTA. Hairpin densities in these samples were lower than in samples implanted with BF_2^+ at room temperature. However, samples which received a furnace heat treatment at 500° C (1 h) prior to RTA were found to contain high densities of hairpins ($5\text{-}10 \times 10^7$ cm^{-2}) following annealing. These results suggest that modifications occuring in the amorphous-crystalline (α/c) transition region during both furnace annealing at moderate temperature ($\sim$500° C) and (nominal) room temperature BF_2^+-implantation are responsible for the creation of high densities of hairpin nucleation sites.

Samples pre-amorphized with Ge^+ were found to contain much lower densities of hairpin dislocations. For example, the hairpin density in silicon pre-amorphized with Ge^+ at LN_2 temperature and then rapid-thermally-annealed was estimated to be $\lesssim 10^6$ cm^{-2} from plan-view and XTEM images. As shown in ref. (13), the primary structural difference between Si^+ and Ge^+-pre-amorphized silicon is the width of the α/c transition region; the transition region in self-implanted

silicon is broad (20-150nm) whereas the α/c transition region in Ge^+-implanted silicon is very narrow ($\lesssim$10 nm). It will be shown in the following sections that the structure of this α/c transition region plays a key role in the hairpin nucleation process.

Geometry of Hairpin Dislocations

The Burgers vectors and arm directions of hairpin dislocations were determined by tilting experiments on plan-view and XTEM specimens. The geometry of a typical hairpin dislocation after RTA at 1150° C for 10 seconds is illustrated in Fig. 2. Note that the hairpins are perfect dislocations with Burgers vectors ($\vec{b}$ = a/2<101>) inclined by 45° to the sample surface. For low RTA temperatures ($\lesssim$ 950° C), the tips of the hairpins are located at a depth which corresponds to the upper portion of the α/c transition region before annealing ($\sim$0.6-0.7 μm)(7,8). During annealing at higher temperatures the hairpin tips glide toward the sample surface (see Fig. 1(c)). Thus, the hairpin shape projected along the Burgers vector remains unchanged.

Nucleation of Hairpin Dislocations

Figure 3(a) shows a cross-section of the α/c transition region in a Si^+-pre-amorphized sample subsequently implanted at (nominal) room temperature with BF_2^+. The α/c transition region is very broad ($\sim$0.12 μm). The high magnification image (Fig. 3(b)) reveals the presence of misoriented crystallites surrounded by amorphous material near the upper portion of the transition region at a depth of $\sim$0.7 μm. The misorientation is thought to be a result of stresses in the transition region which result from the difference in density (15) between amorphous and crystalline silicon.

Based upon these images and the results of the previous section, the following model for nucleation of a hairpin dislocation is proposed (Fig. 4): During RTA, the advancing and recrystallizing α/c growth front intersects a small misoriented crystallite in the upper portion of the α/c transition region. A perfect dislocation segment is formed at the intersection to accommodate the misorientation. As the combined growth front continues to move, the dislocation segment wraps around the misoriented material to form a half loop. The growth front emanating from the misoriented material remains slightly ahead of the surrounding primary growth front. Verification of this growth front morphology is provided by the XTEM image of the partially regrown sample (750° C, 10 sec) shown in Fig. 5.

As the annealing continues, the hairpin arms diverge since the growth front protrusion of misoriented material is spreading laterally as well as vertically. During further annealing the dislocation shortens its length by moving toward the surface along the glide cylinder defined by the inclined Burgers vector and line direction.

It is clear from this model and the results above that a broad transition region contains a high density of misoriented crystallites, thereby resulting in the nucleation of a high density of hairpin dislocations. Thus, the above model also explains the observation that Ge^+-pre-amorphized samples with very narrow α/c transition regions contain a much lower density of hairpin dislocations following RTA.

Conclusions

Based upon the XTEM results, a simple model for the nucleation of hairpin dislocations during RTA of pre-amorphized silicon has been

proposed. From this model and the results presented above, it is evident that the nucleation of high densities ($\gtrsim 10^7$ cm^{-2}) of hairpin dislocations cannot be avoided unless the α/c transition region is sufficiently narrow ($\lesssim 30$ nm). Consequently, if Si^+-pre-amorphization is to be employed in the fabrication of very shallow p^+-n junctions as a technique for channeling suppression, the pre-amorphization and subsequent implantation steps (prior to RTA) should be accomplished at low substrate temperatures ($\lesssim LN_2T$). Alternatively, the narrow (typically $\lesssim$10nm) α/c transition region produced by heavy ion (e.g. Ge^+ or As^+) implantation contains a much lower density of potential nucleation sites (misoriented crystallites). Thus, a simpler and more effective method to limit hairpin nucleation during RTA is to pre-amorphize by single-step implantation of Ge^+ at either LN_2 or room temperature.

Acknowledgements

The authors would like to thank Dr. Ulrich Dahmen for useful discussions, and the staff of the National Center for Electron Microscopy, Lawrence Berkeley Laboratory, for technical assistance. This work was supported by the Director, Office of Energy Research, Office of Basic Energy Sciences, Materials Sciences Division of the U.S. Department of Energy under Contract No. DE-AC03-76SF00098 and the Semiconductor Research Corporation.

References

1. W.K. Hofker, Philips Res. Rep. Suppl. (8); Philips, Eindhoven, 1975.
2. R.G. Wilson, J. Appl. Phys., 54 (1983) p. 6879.
3. T.-Y. Liu, Ph.D. Thesis, University of California, Berkeley, (1983), Ch. 5.
4. B.L. Crowder, J.F. Ziegler and G.W. Cole, p. 257 in Ion Implantation in Semiconductors and Other Materials, B.L. Crowder, ed.; Plenum, New York, N.Y., 1973.
5. M.Y. Tsai and B.G. Streetman, J. Appl. Phys., 50 (1979) p. 183.
6. T.E. Seidel, IEEE Electron Dev. Lett., EDL-4 (10) (1983) p. 353.
7. W. Maszara, C. Carter, D.K. Sadana, J. Liu, V. Ozguz, J. Wortman and G.A. Rozgonyi, in Proc. of Mat. Res. Soc.; Energy Beam-Solid Interactions and Transient Thermal Processing, J.C.C. Fan and N.M. Johnson, eds.; North-Holland, New York, N.Y., 1984.
8. C. Carter, W. Maszara, D.K. Sadana, G.A. Rozgonyi, J. Liu and J. Wortman, Appl. Phys. Lett., 44 (1984) p. 459.
9. T.E. Seidel, R.W. Knoell, F.A. Stevie, G. Poli, B. Schwartz, p. 201 in VLSI Science and Technology/1984, Bean and Rozgonyi, eds., The Electrochemical Society, Vol. 84-7, 1984.
10. D.K. Sadana, W. Maszara, J.J. Wortman, G.A. Rozgonyi and W.K. Chu, J. Electrochem Soc., 131 (1984) p. 943.
11. D.K. Sadana, E. Myers, J. Liu, T. Finstead and G.A. Rozgonyi in Proc. of Mat. Res. Soc.; Energy Beam-Solid Interactions and Transient Thermal Processing, J.C.C. Fan and N.M. Johnson, eds.; North-Holland, New York, N.Y., 1984.

12. T. Sands, J. Washburn, R. Gronsky, W. Maszara, D.K. Sadana and G.A. Rozgonyi, Appl. Phys. Lett. (1984) in press.

13. T. Sands, J. Washburn, E. Myers and D.K. Sadana, in Proc. of Ion Beam Mod. of Mat. Conf., Nuc. Inst. and Methods - B. J. Mayer, ed. 1984, in press.

14. T.E. Seidel, in Proc. of Ion Beam Mod. of Mat. Conf., Nuc. Inst. and Methods - B. J. Mayer, ed. 1984, in press.

15. J. Wilson, Metal Rev., 10 (1965) 381.

Figure Captions

Fig. 1. Comparison of XTEM images ($\vec{g}$ = 220) and SIMS fluorine profiles for Si^+-pre-amorphized, BF_2^+-implanted and rapid-thermally-annealed silicon. Note that during RTA at 950°C for 10 sec. fluorine is gettered to hairpin tips and interstitial loops resulting in double fluorine peak.

Fig. 2. Stereographic projection indicating geometry of typical hairpin dislocation after RTA at 1150°C for 10 sec. The appearance of this hairpin dislocation as observed by XTEM is schematically illustrated for the three zone-axis directions $[0\bar{1}0]$, $[1\bar{1}0]$ and [100].

Fig. 3. a) Cross-sectional image in <110> zone-axis orientation of the α-c transition region in Si^+-pre-amorphized and BF_2^+-implanted (at RT) silicon. b) High magnification image of boxed region in (a) showing microcrystalline islands. Misoriented crystallites are located at depth of $\sim$0.7 μm from surface.

Fig. 4. Schematic diagram illustrating model for hairpin nucleation during RTA(see text for description). Viewing direction is approximately [010] (see Fig. 2). Note that hairpin is approximately edge-on in this projection.

Fig. 5. Cross-sectional image in <110> zone-axis orientation of sample in Fig. 3 after RTA at 750°C for 10 sec. Regrowth is only partially complete, leaving band of amorphous material 450 nm wide. Note that growth front between hairpin arms is slightly ahead of primary growth front. Small defects below $\sim$700 nm become interstitial loops after further annealing (see Fig. 1(a,c)).

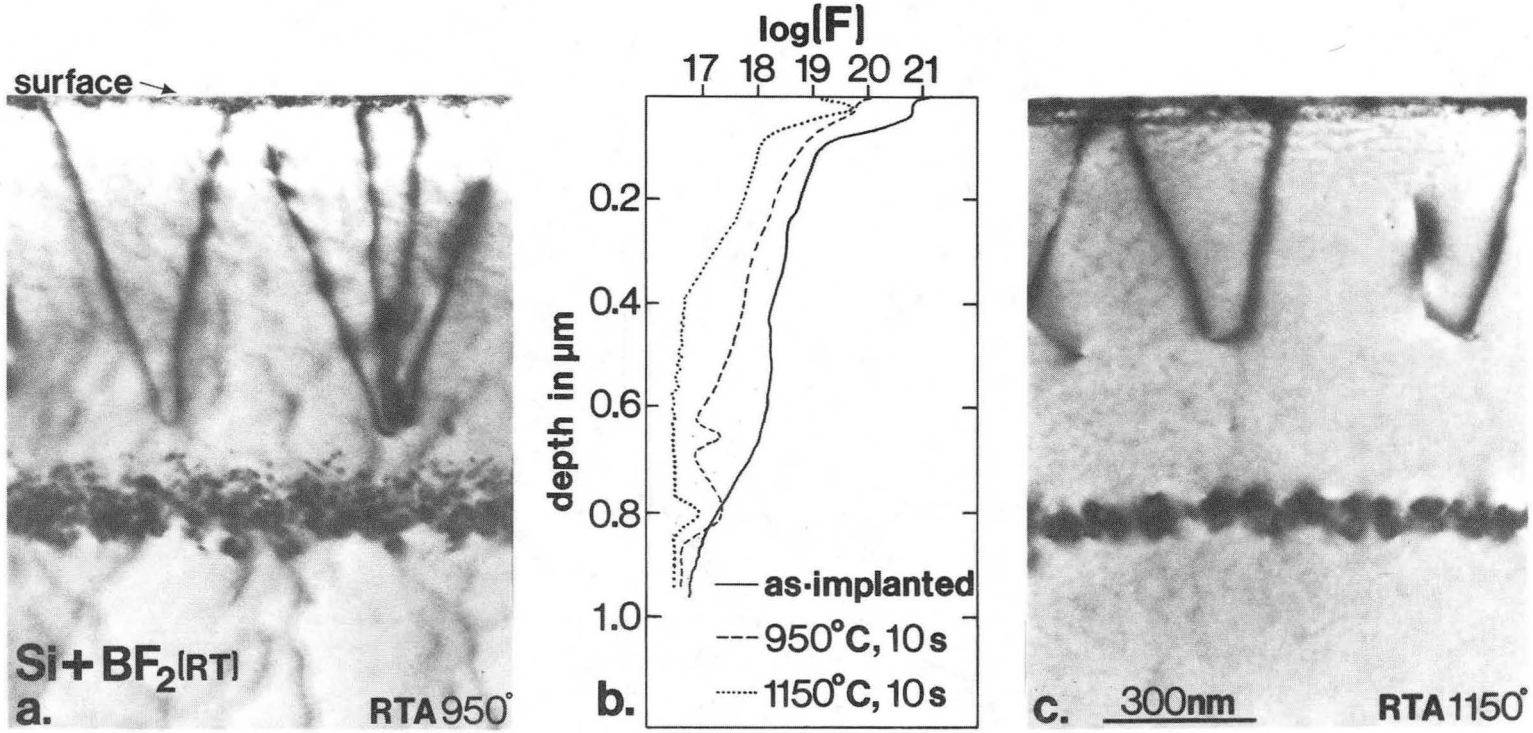

XBB 847-5431

Fig. 1

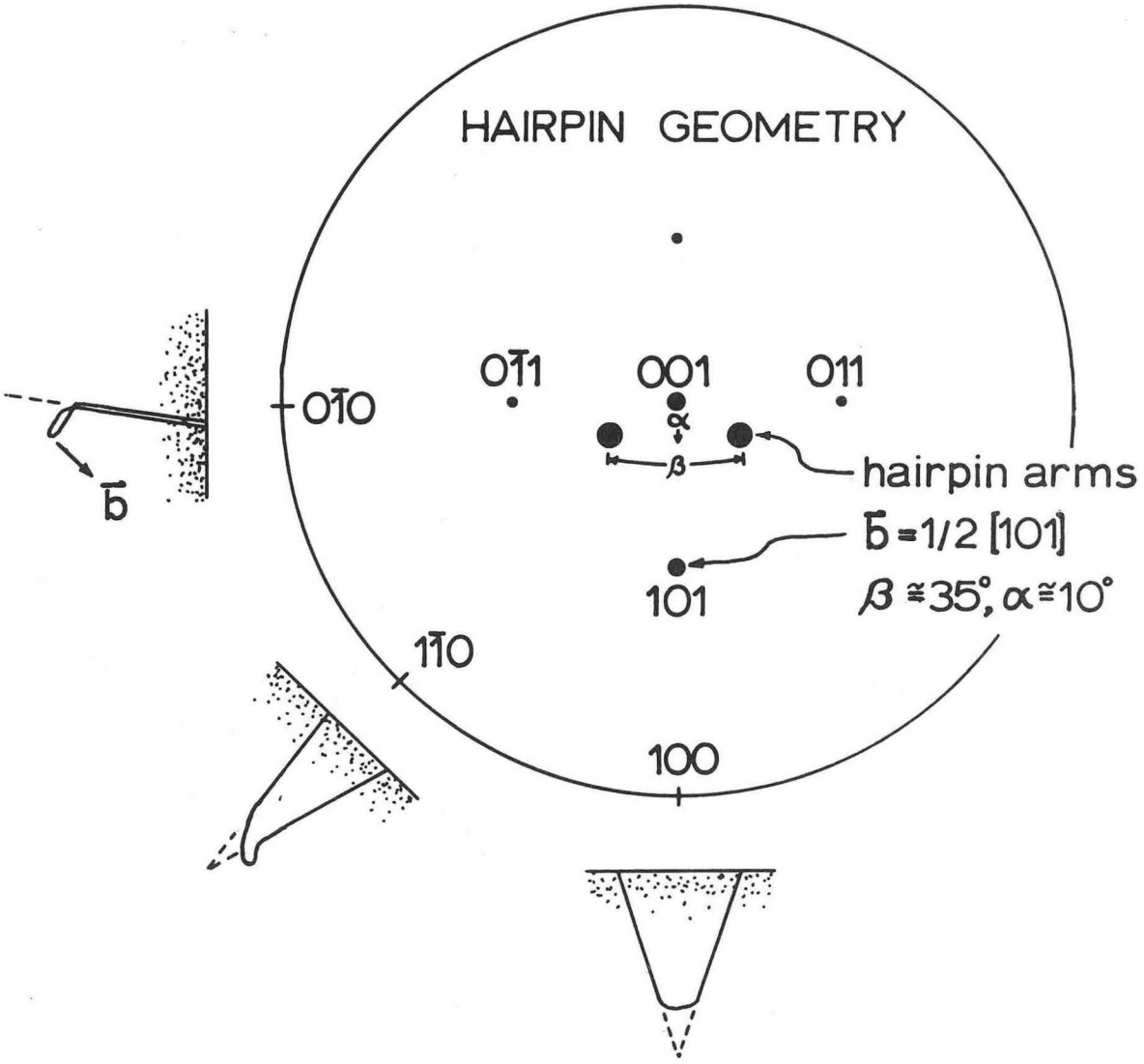

XBL 845-1922

Fig. 2

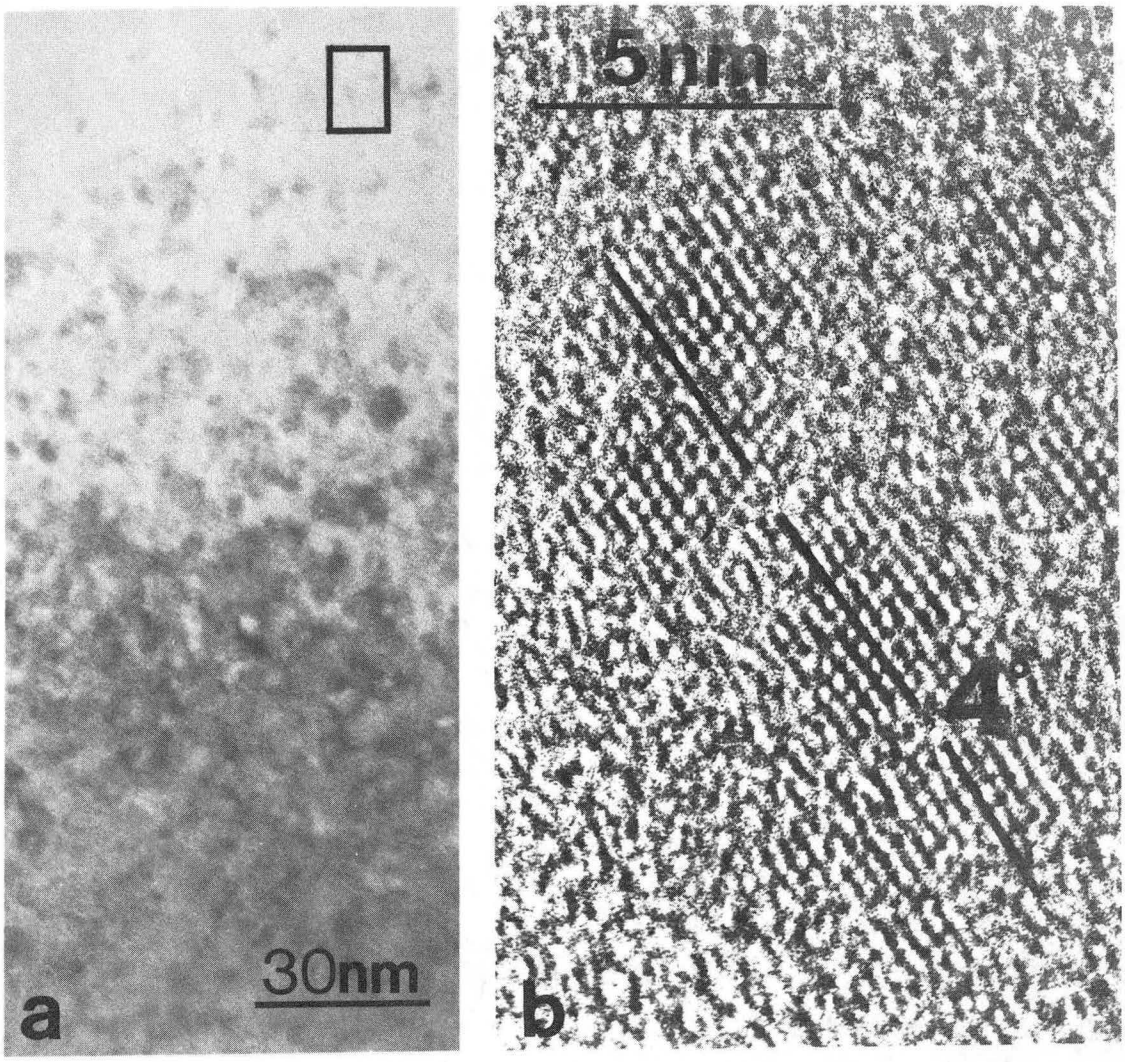

XBB 847-5493

Fig. 3

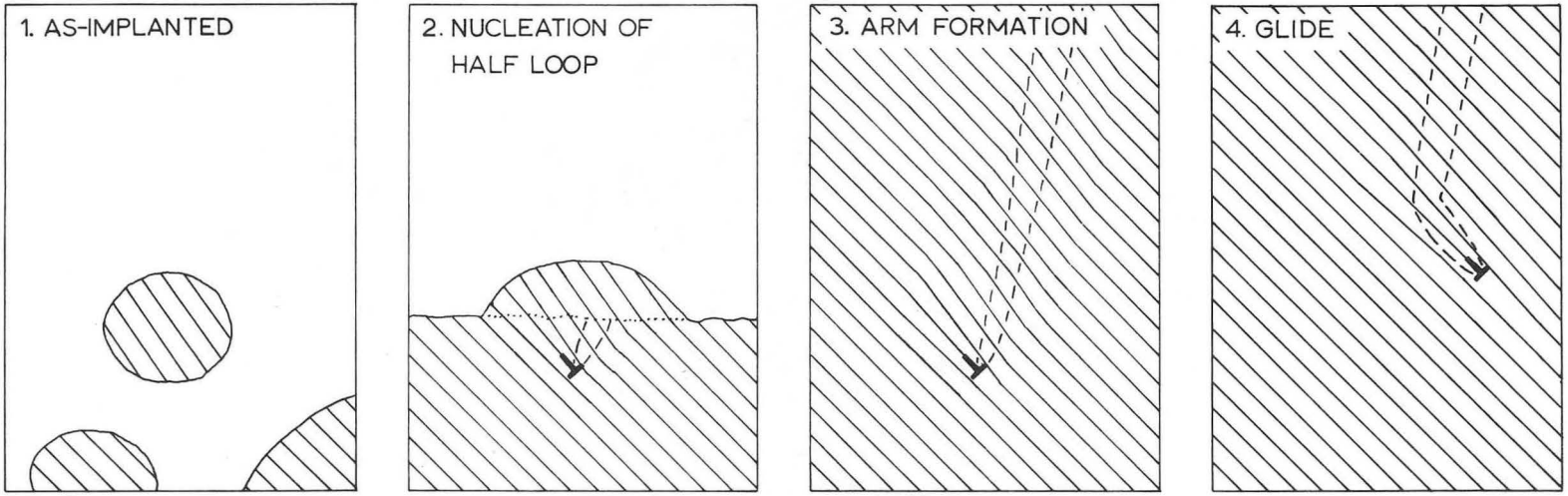

XBL 847-3147

Fig. 4

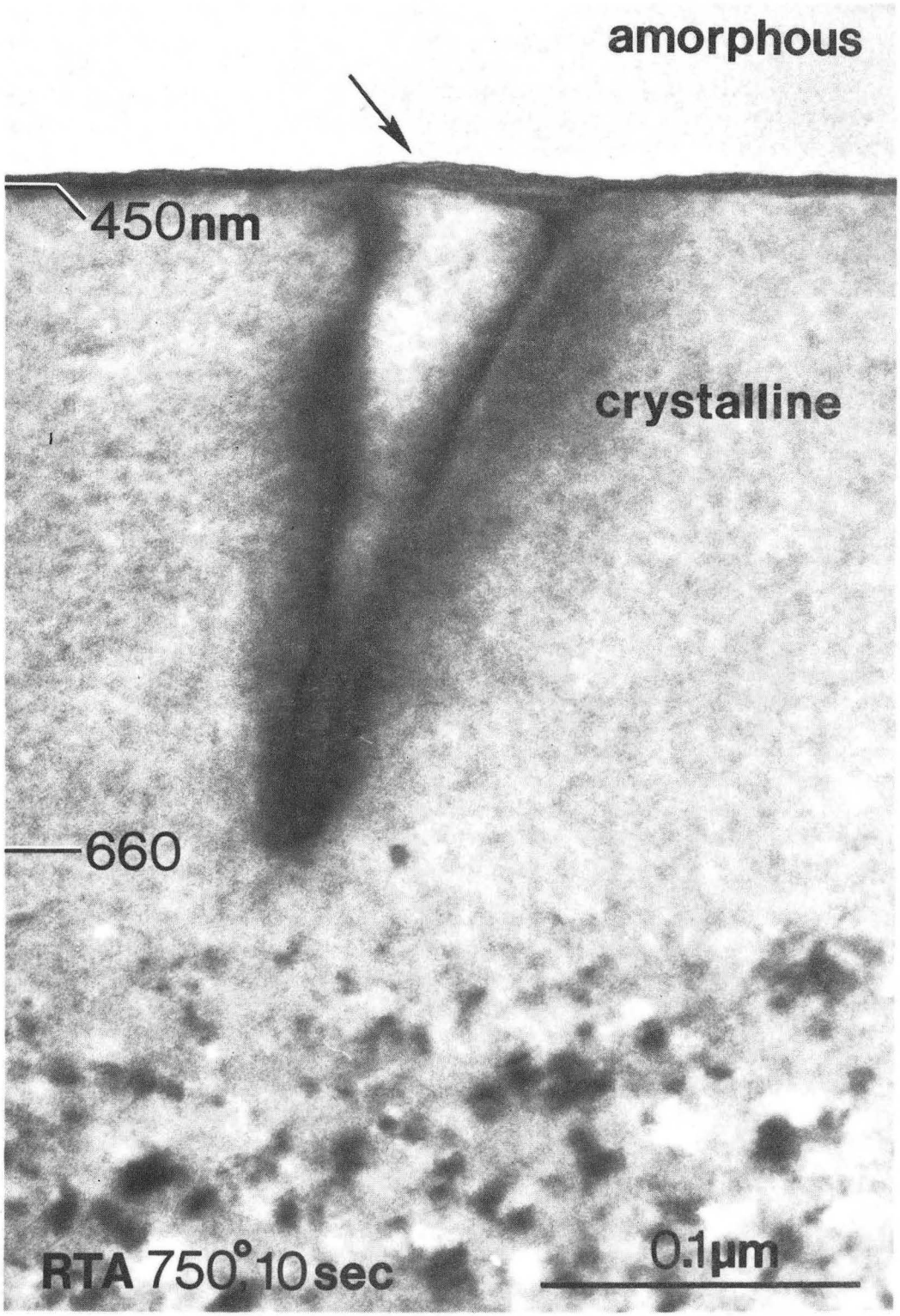

XBB 847-5430

Fig. 5

This report was done with support from the Department of Energy. Any conclusions or opinions expressed in this report represent solely those of the author(s) and not necessarily those of The Regents of the University of California, the Lawrence Berkeley Laboratory or the Department of Energy.

Reference to a company or product name does not imply approval or recommendation of the product by the University of California or the U.S. Department of Energy to the exclusion of others that may be suitable.

TECHNICAL INFORMATION DEPARTMENT
LAWRENCE BERKELEY LABORATORY
UNIVERSITY OF CALIFORNIA
BERKELEY, CALIFORNIA 94720